

# Compressive Hyperspectral Imaging by Out-of-Focus Modulations and Fabry-Pérot Spectral Filters

K. Degraux<sup>1</sup>, V. Cambareri<sup>2</sup>, B. Geelen<sup>3</sup>, L. Jacques<sup>1</sup>, G. Lafruit<sup>3</sup> and G. Setti<sup>2</sup>.

<sup>1</sup>ISPGROUP/ICTEAM, Université catholique de Louvain, Belgium. <sup>2</sup>ARCES, University of Bologna, Italy. <sup>3</sup>IMEC, Belgium.

**Abstract**— We describe a compressive hyperspectral imaging scheme that randomly convolves each spectral band of the data cube. This independent sensing of each wavelength relies on a tiling of Fabry-Pérot filters incorporated in the CMOS pixel grid. The compressive observations are induced by an out-of-focus spatial light modulation joined to focusing optics. While our design extends a recent monochromatic imaging scheme to the hyperspectral domain, we show that our model reaches good reconstruction performances when compared to more ideal sensing methods.

## 1 Introduction

Hyperspectral imaging is an advanced imaging technique which integrates spectroscopy into the image capturing process, providing for each pixel its light intensity as a function of wavelength. The resulting information is organized into a *hyperspectral* (HS) cube with two spatial and one spectral dimensions, which may be interpreted as a stack of images, one for each wavelength. Spectral cameras are currently used in research applications such as remote sensing [1] and food inspection [2], where this detailed spectral information may be used at application-level to identify objects and materials. Due to rapidly falling system complexity, size and cost, such technologies are expected to be adopted in more general purpose applications [3].

In order to acquire these vast amounts of data, spectral cameras typically use a time-consuming scanning approach, based on, *e.g.*, line scanning with dispersive optics (such as prisms and gratings [4]) or spectral scanning using tunable filters (*e.g.*, AOTF [5]). This problem may be overcome using snapshot acquisition, where the entire 3-D datacube is acquired during one frame period by optically *multiplexing* the contents of the 3-D cube onto a 2-D sensor. Whereas in scanning spectral imaging the data in a spectral cube is conveyed to multiple, consecutive frames, in snapshot spectral imaging this data is multiplexed onto a single frame of the sensor. However, due to the limited number of sensor pixels, snapshot imagers require a trade-off between spatial and spectral resolution.

This trade-off has been previously tackled by using *compressive sensing* (CS) techniques [6] to acquire the 3-D HS cube at sub-Nyquist sampling rates [7, 8]. In this work, we introduce a new compressive HS scheme that combines a snapshot imaging sensor based on monolithically integrated Fabry-Pérot [9] filter tiles with an optical front-end based on an out-of-focus spatial light modulator (SLM). By allowing the number of SLM patterns to vary at runtime, the system can reach higher SNR, thus operating as a hybrid setup between a scanning and a snapshot spectral camera. Since compressive sensing techniques avoid scanning, associated problems with motion blur and reduced SNR in high speed applications are also avoided.

## 2 Optical and Sensing Model

In this work, we extend the monochromatic compressive optical scheme developed by Björklund and Magli [10] for acquir-

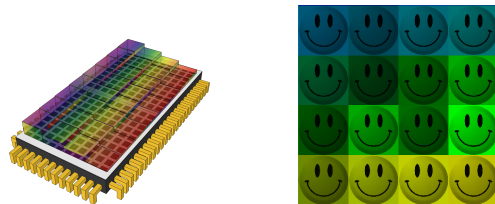


Fig. 1: (left) Tiled Fabry-Pérot filters on top of a CMOS sensor. (right) Part of a tiled representation of our low-rank and sparse HS toy example.

ing hyperspectral images. Our imager model is actually built around a snapshot spectral sensor, which monolithically integrates a set of Fabry-Pérot (FP) interferometers organized as tiled filters on top of a standard, off-the-shelf CMOS sensor [3] (Fig. 1). The FP filter is typically made of a transparent layer (or *cavity*) with two mirrors at each side of that layer. The cavity length and the mirror reflectivity determine the selected wavelength and the spectral bandwidth (or *full width at half maximum*) of the filter, respectively. Thanks to the monolithic integration of the filter on the sensor, the stray light in the system is heavily reduced and the sensitivity and the speed of the sensor are increased [11]. The use of CMOS process technology heavily reduces the cost and improves the compactness of the hyperspectral camera.

Let us now explain how the FP filters are combined with the compressive setup. The optical model of the imager, restricted to a 2-D section for simplicity, is illustrated in Fig. 2 (a). First, in a *monochromatic* setting, an object is imaged by conventional *objective* optics  $O$  on an *image plane*. Classical optics tells us that every point on this plane radiates light in many directions, as initially produced by the original object point. Therefore, after the image plane, the object image is replicated in many *beams* of parallel light rays. By placing an out-of-focus *spatial light modulator* (SLM) after that plane, each of such beams can be modulated differently according to its direction, before being focused (*i.e.*, “summed”) on a single pixel of the detector by a second lens  $F$ . If this lens has focal length  $f$ , this pixel is located at distance  $f \tan \theta$  of the optical axis. By construction, the detector actually records specific samples of the *convolution* (up to a kernel reversal) between the image and the modulation. In the case of *polychromatic* imaging with no chromatic aberrations in our optics<sup>2</sup>, by tiling the detector with FP spectral filters we independently convolves different slices of the HS volume with the SLM modulation. As explained hereafter, by inserting a random SLM pattern, the optical scheme can compressively image the HS volume, wavelength-wise, with a partial Toeplitz sensing [12].

Mathematically, let a HS volume  $\mathbf{x} \in \mathbb{R}^{N \times N \times L^2}$  with  $N_{\text{tot}} = L^2 N^2$  voxels to be acquired by the imager. The number of wavelengths is set to a square value  $L^2$  since the detector is made of a 2-D grid of  $N_s \times N_s$  pixels covered by a grid of  $L \times L$  square tiles  $\mathcal{T}_j$  ( $1 \leq j \leq L^2$ ) of distinct FP filters, each selecting one wavelength  $\lambda_j$ . Assuming  $N_s$  divisible by  $L$ , each tile spectrally filters the light received by a square patch of

We thank the supercomputing facilities (CISM/UCL) and the CECL, funded by FRS-FNRS, for their computational resources. LJ and KD are funded by the FRS-FNRS.

<sup>2</sup>These will be fully considered in a future study.

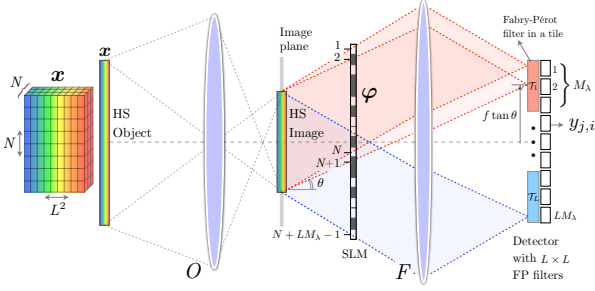


Fig. 2 (a): The compressive hyperspectral imager (1-D slice)

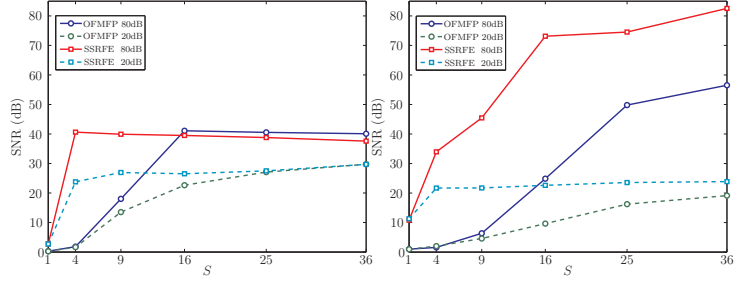


Fig. 2 (b): Low-rank/joint sparsity model.

Fig. 2 (c): Total variation model.

$M_\lambda \times M_\lambda$  pixels, with  $M_\lambda = N_s/L$ . By design (see Fig. 2 (a)), since any replication of the image must be spatially modulated at resolution  $N$  (so as to determine the spatial resolution of  $\mathbf{x}$ ) and by adjusting a shift of one pixel in the detector to a shift of one pixel for the associated image beam in the SLM plane, we have  $N_{\text{slm}} = N + N_s - 1 = N + LM_\lambda - 1$ . For limiting the SLM resolution, we arbitrary set  $N_{\text{slm}} = 2N - 1$  so that  $N_s = N$  and  $M_\lambda = N/L$ .

Every pixel of a given tile  $\mathcal{T}_j$  is influenced by a limited part  $\varphi_j \in \mathbb{R}^{(N+M_\lambda) \times (N+M_\lambda)}$  of the whole SLM modulation  $\varphi \in \mathbb{R}^{N_{\text{slm}} \times N_{\text{slm}}}$ . Therefore, denoting by  $\bar{\mathbf{w}}$  the *vectorization* of any matrix  $\mathbf{w}$ , the recorded light intensities  $\mathbf{y}_j \in \mathbb{R}^{M_\lambda \times M_\lambda}$  in  $\mathcal{T}_j$  read

$$\bar{\mathbf{y}}_j = \Phi_j \bar{\mathbf{x}}_j + \bar{\mathbf{n}}_j \in \mathbb{R}^{M_\lambda^2}, \quad \Phi_j := \mathbf{S}_j \mathbf{C}_j,$$

where  $\bar{\mathbf{x}}_j$  is the  $j^{\text{th}}$  slice of  $\mathbf{x}$  at wavelength  $\lambda_j$ ,  $\mathbf{C}_j \in \mathbb{R}^{N^2 \times N^2}$  is the Toeplitz matrix convolving an input image with  $\varphi_j$ ,  $\mathbf{S}_j \in \{0, 1\}^{M_\lambda^2 \times N^2}$  is a selection matrix extracting indices associated to pixels in  $\mathcal{T}_j$ , and  $\bar{\mathbf{n}}_j$  accounts for possible measurement noise. Gathering all the wavelengths and vectorizing the result, the whole sensing model is  $\bar{\mathbf{y}} = \Phi \bar{\mathbf{x}} + \bar{\mathbf{n}}$ , with  $\Phi := \text{diag}(\Phi_1, \dots, \Phi_{L^2})$  and  $\mathbf{y}, \mathbf{n} \in \mathbb{R}^{M_\lambda \times M_\lambda \times L^2}$ .

The final sensing is thus realized independently for each wavelength, as observed from the block structure of  $\Phi$ . This restricts the performances of our system compared to an ideal compressive imaging device, *i.e.*, when  $\Phi$  is dense and unstructured. However, conversely to the sensing operator, the reconstruction methods recovering  $\mathbf{x}$  from  $\mathbf{y}$  as described in Sec. 3 exploit the 3-D structure of the data.

Compressed Sensing theory [6] shows that if a  $M \times D$  sensing matrix  $\mathbf{A}$  respects the *restricted isometry property* (RIP) with sufficiently small RIP constant, any  $K$ -sparse (or compressible) signals of  $\mathbb{R}^D$  can be recovered (or estimated) from the possibly noisy measurement vector  $\mathbf{A}\mathbf{x} \in \mathbb{R}^M$ . Moreover, a structured sensing issued from a  $M$ -subsampled Toeplitz or circulant matrix whose generating entries are drawn from an iid Bernoulli  $\pm 1$  distribution, satisfies the restricted isometry property (RIP) on  $K$ -sparse signals if  $M \geq M_0 = O(K^{3/2}(\log D)^{3/2})$  [12]. Since the matrices  $\Phi_j$  respect such a Toeplitz structure (even in 2-D), we can therefore expect to efficiently reconstruct each slice of the HS volume  $\mathbf{x}$  under a sparse signal prior provided the number of observations is large. However, this work tests the regularizing capabilities of two other priors: a 3-D *total variation* (TV), for a ‘‘cartoon shape’’ HS model, and a low-rank and joint sparse prior [13].

We also consider a situation where the number  $M_\lambda^2 = N^2/L$  of observations per band for one modulation  $\varphi$  is fixed by the detector design. An increasing number of observations is reached by merging the measurements obtained for  $S$  different random SLM patterns. The HS volume  $\mathbf{x}$  of  $N^2 L^2$  voxels is thus observed with a total of  $M_\lambda^2 L^2 S = N^2 S$  measurements, *i.e.*, we

aim at reaching  $1 \leq S \ll L^2$  with high reconstruction quality.

### 3 Simulations

The capability of our HS imaging scheme has been simulated as follows. We focus our study on two toy examples of size  $N = 256$  and  $L = 8$ , *i.e.*, two structured HS volumes with  $N_{\text{tot}} = 2^{22}$  voxels. The first is a ‘‘Mondrian-like’’ example [15] with small 3-D *total variation* (TV) [14] made of 8 randomly generated overlapping cubes of different sizes and values in the HS volume. The second example follows a low-rank source model (LRSM) of rank  $r = 4$  with (joint) sparsity level  $K = N^2/16 = 4096$  [13] (see Fig. 1).

Two kinds of reconstruction methods have been used to recover these HS volumes from their compressive observations. For the ‘‘Mondrian’’ example, we solve  $\mathbf{x}^* = \text{argmin}_{\mathbf{u}} \|\mathbf{u}\|_{TV} + \rho \|\mathbf{y} - \Phi \mathbf{u}\|_2^2$  thanks to the TwIST algorithm [16] and by manually adjusting  $\rho$ . The recovery of the LRSM example is achieved by promoting a low-rank and joint sparse data model [13], *i.e.*,

$$\mathbf{x}^* = \text{argmin}_{\mathbf{u}} (\sum_j \|\Psi^T \bar{\mathbf{u}}_j\|_1^2)^{1/2} + \rho \|(\bar{\mathbf{u}}_1, \dots, \bar{\mathbf{u}}_{L^2})\|_*$$

s.t.  $\|\mathbf{y} - \Phi \mathbf{u}\|_2 \leq \epsilon,$

where  $\|\mathbf{A}\|_*$  is the trace norm of  $\mathbf{A}$ ,  $\Psi^T$  is the spatial Haar wavelet transform [17] at every wavelength, and the first term in the minimized cost is the  $\ell_1/\ell_2$  mixed norm enforcing *joint* sparsity at every wavelength [18]. This optimization problem is solved by proximal algorithms [19, 20] with  $\rho = \sqrt{K/2r}$  [13].

Fig. 2 (b) and Fig. 2 (c) display the reconstruction SNR for both methods as a function of the number of random SLM patterns  $S$ . Two noisy sensing scenarios were considered with measurement noise at 20 and 80 dB. The sensing associated to our out-of-focus modulation with FP filters (OFMFP) is confronted with the more efficient spread-spectrum random Fourier ensemble (SSRFE) sensing [21], also applied bandwise. For the two noise levels and the two considered HS examples, we see that our sensing quickly reaches similar reconstruction qualities as SSRFE for increasing  $S$ , with a stronger match for the LRSM model. Moreover, for these two toy examples and under a 20 dB noise, as soon as  $S \gtrsim 16$  (*i.e.*, 25% of Nyquist rate), the SNR starts to saturate to a value related to the noise power.

### 4 Discussions and Conclusion

The capability of a compressive HS imager combining a CMOS detector tiled with FP filters and an out-of-focus SLM modulation has been studied. Despite an independent sensing of each wavelength, our simulations demonstrate already good performances on toy examples for a small number of modulations compared to the number of wavelengths. In a future work, the optical aberrations of the different optics and the SLM diffraction will be integrated in the sensing model. We will also study how to modulate the cube both spatially and spectrally.

## References

- [1] P. Shippert “Why use Hyperspectral Imagery,” *Photogrammetric Engineering and Remote Sensing*, **70**(4): 377–380, 2004.
- [2] A. A. Gowen, C.P. O’Donnell, P.J. Cullen, G. Downey and J.M. Frias, “Hyperspectral imaging - an emerging process analytical tool for food quality and safety control,” *Trends in Food Science and Technology*, **18**(12): 590–598, 2007.
- [3] N. Tack, A. Lambrechts, S. Soussan and L. Haspeslagh, “A compact, high-speed, and low-cost hyperspectral imager,” *Proc. SPIE 8266, Silicon Photonics VII* (2012).
- [4] “Inspector Fast”: <http://www.specim.fi/media/inspector-datasheets/inspector-fast10-ver1-11.pdf>
- [5] N. Gupta, R. Dahmani, K. Bennett, S. Simizu, R. Dennis and N.B. Singh, “Progress in AOTF hyperspectral imagers,” *Proc. SPIE Vol. 4054*, 30–38 (2000).
- [6] E. Candès, J. K. Romberg, T. Tao, “Stable signal recovery from incomplete and inaccurate measurements”, *Communications on Pure and Applied Mathematics*, **59**(8):1207–1223, 2006.
- [7] M.E. Gehm, R. John, D. J. Brady, R. M. Willett, and T. J. Schulz, “Single-shot compressive spectral imaging with a dual-disperser architecture,” *Opt. Express*, **15**(21):14013–14027, 2007.
- [8] H. Arguello and G. R. Arce, “Code aperture optimization for spectrally agile compressive imaging”, *JOSA A* **28**(11):2400–2413, 2011.
- [9] The Fabry-Pérot resonator, Dickmann: <http://repairfaq.ece.drexel.edu/sam/MEOS/EXP03.pdf>
- [10] T. Björklund and Enrico Magli, “A Parallel Compressive Imaging Architecture for One-Shot Acquisition”, 30th Picture Coding Symposium (PCS 2013). arXiv preprint arXiv:1311.0646 (2013).
- [11] J. Loesel and D. Laubier, “Study of accessible performances of a spectro imager using a wedge filter,” *Proc. of SPIE*, 7100, (2008).
- [12] H. Rauhut, J. Romberg and J. A. Tropp, “Restricted isometries for partial random circulant matrices.” *Applied and Computational Harmonic Analysis* **32**(2):242–254, 2012.
- [13] M. Golbabaee and P. Vandergheynst, “Compressed Sensing of Simultaneous Low-Rank and Joint-Sparse Matrices”, submitted to *IEEE Transactions on Information Theory*, p. 32, 2012.
- [14] L. I. Rudin, S. Osher and E. Fatemi, “Nonlinear total variation based noise removal algorithms,” *Physica D: Nonlinear Phenomena* **60**(1):259–268, 1992.
- [15] M. J. Fadili and J-L. Starck, “Monotone operator splitting for optimization problems in sparse recovery,” 16th IEEE International Conference on Image Processing (ICIP), pp.1461–1464, 2009.
- [16] J. Bioucas-Dias and M. Figueiredo, “A new TwIST: two-step iterative shrinkage/thresholding algorithms for image restoration”, *IEEE Transactions on Image Processing*, **16**(12): 2992–3004, 2007.
- [17] G. Peyré, “The Numerical Tours of Signal Processing - Advanced Computational Signal and Image Processing,” *IEEE Computing in Science and Engineering*, **13**(4):94–97, 2011.
- [18] M. Kowalski, “Sparse regression using mixed norms,” *Applied and Computational Harmonic Analysis*, **27**(3):303–324, 2009.
- [19] P. L. Combettes and J.-C. Pesquet, “Proximal splitting methods in signal processing”, *Fixed-Point Algorithms for Inverse Problems in Science and Engineering*. Springer New York, pp. 185–212, 2011.
- [20] A. Chambolle and T. Pock “A first-order primal-dual algorithm for convex problems with applications to imaging” *Journal of Mathematical Imaging and Vision* **40**(1):120–145, 2011.
- [21] G. Puy, P. Vandergheynst, R. Gribonval, and Y. Wiaux, “Universal and efficient compressed sensing by spread spectrum and application to realistic Fourier imaging techniques,” *EURASIP Journal on Advances in Signal Processing*, vol. 2012, pp. 1-13, 2012.